

The upper critical field and its anisotropy in $(\text{Li}_{1-x}\text{Fe}_x)\text{OHFe}_{1-y}\text{Se}$

This content has been downloaded from IOPscience. Please scroll down to see the full text.

2017 J. Phys.: Condens. Matter 29 025701

(<http://iopscience.iop.org/0953-8984/29/2/025701>)

View [the table of contents for this issue](#), or go to the [journal homepage](#) for more

Download details:

IP Address: 159.226.35.181

This content was downloaded on 15/11/2016 at 10:47

Please note that [terms and conditions apply](#).

You may also be interested in:

[Pressure dependence of upper critical fields in FeSe single crystals](#)

Ji-Hoon Kang, Soon-Gil Jung, Sangyun Lee et al.

[Transport properties and anisotropy of superconducting \$\(\text{Li}_{1-x}\text{Fe}_x\)\text{OHFeSe}\$ single crystals](#)

Chunlei Wang, Xiaolei Yi, Yang Qiu et al.

[From Kondo lattices to Kondo superlattices](#)

Masaaki Shimosawa, Swee K Goh, Takasada Shibauchi et al.

[An overview of the Fe-chalcogenide superconductors](#)

M K Wu, P M Wu, Y C Wen et al.

[Upper critical field, lower critical field and critical current density of \$\text{FeTe}_{0.60}\text{Se}_{0.40}\$ single crystals](#)

C S Yadav and P L Paulose

[Tunnel diode oscillator measurements of the upper critical magnetic field of \$\text{FeTe}_{0.5}\text{Se}_{0.5}\$](#)

A Audouard, L Drigo, F Duc et al.

[Superconducting properties of iron chalcogenide thin films](#)

Paolo Mele

The upper critical field and its anisotropy in $(\text{Li}_{1-x}\text{Fe}_x)\text{OHFe}_{1-y}\text{Se}$

Zhaosheng Wang¹, Jie Yuan², J Wosnitzer¹, Huaxue Zhou², Yulong Huang², Kui Jin², Fang Zhou², Xiaoli Dong² and Zhongxian Zhao²

¹ Hochfeld-Magnetlabor Dresden (HLD-EMFL), Helmholtz-Zentrum Dresden-Rossendorf, D-01314 Dresden, Germany

² Beijing National Laboratory for Condensed Matter Physics, Institute of Physics, Chinese Academy of Sciences, Beijing 100190, People's Republic of China

E-mail: z.wang@hzdr.de

Received 21 July 2016, revised 24 October 2016

Accepted for publication 25 October 2016

Published 14 November 2016



CrossMark

Abstract

The temperature dependence of the upper critical field (H_{c2}) in a $(\text{Li}_{1-x}\text{Fe}_x)\text{OHFe}_{1-y}\text{Se}$ single crystal ($T_c \approx 40$ K) has been determined by means of magnetotransport measurements down to 1.4 K both for inter-plane ($H\parallel c$, $H_{c2}^{\parallel c}$) and in-plane ($H\parallel ab$, $H_{c2}^{\parallel ab}$) field directions in static magnetic fields up to 14 T and pulsed magnetic fields up to 70 T. $H_{c2}^{\parallel c}$ exhibits a quasilinear increase with decreasing temperature below the superconducting transition and can be described well by an effective two-band model with unbalanced diffusivity, while $H_{c2}^{\parallel ab}$ shows a flattening below 35 K and follows the Werthamer–Helfand–Hohenberg (WHH) model incorporating orbital pair-breaking and spin-paramagnetic effects, yielding zero-temperature critical fields of $H_{c2}^{\parallel c}(0) \approx 67$ T and $H_{c2}^{\parallel ab}(0) \approx 98$ T. The anisotropy of the upper critical fields, $\gamma(T) = H_{c2}^{\parallel ab}/H_{c2}^{\parallel c}$ monotonically decreases with decreasing temperature from about 7 near T_c to 1.5 at 0 K. This reduced anisotropy, observed in most Fe-based superconductors, is caused by the Pauli limitation of $H_{c2}^{\parallel ab}$.

Keywords: Fe-based superconductor, upper critical field, anisotropy

(Some figures may appear in colour only in the online journal)

1. Introduction

Since the discovery of superconductivity at 26 K in the FeAs-based superconductor $\text{LaFeAsO}_{1-x}\text{F}_x$ [1], countless studies investigating the superconducting properties of Fe-based materials were stimulated in the community of condensed matter physicists and materials scientists. As a result, the superconducting transition temperature (T_c) was quickly increased to 55 K [2], making the Fe-based superconductors the second class of high-temperature superconductors. Later, superconductivity was also found in some FeSe-based materials.

β -FeSe shows superconductivity at $T_c \approx 8.5$ K [3, 4]. By adding alkali-metal ions A (K, Cs, Rb, and Tl) between the FeSe layers, higher T_c s above 30 K were successfully achieved [5–9]. However, superconductors of the type $A_y\text{Fe}_{2-x}\text{Se}_2$ always are prone to inhomogeneities and phase separation. The coexistence with an insulating phase suggests that the

interface may play an important role in superconductivity [10–12]. The exact nature of the superconducting phase in these materials still remains unclear. The phase separation and interface effects occurring in $A_y\text{Fe}_{2-x}\text{Se}_2$ hamper well-targeted experimental studies clarifying the origin of high-temperature superconductivity in the Fe-based superconductors. Later, high-temperature superconductivity above 100 K was reported for single-layer FeSe films grown on a SrTiO_3 substrate [13–15]. There are strong indications that the interface in the single-layer FeSe/ SrTiO_3 films plays an important role for the strongly increased transition temperature [15–17].

Recently, the new Fe-based superconductor $(\text{Li}_{1-x}\text{Fe}_x)\text{OHFe}_{1-y}\text{Se}$ (FeSe1111) with T_c up to about 43 K has been synthesized [18–22]. This material consists of FeSe layers sandwiched in between (Li, Fe)OH layers along the c direction. The distance between two adjacent FeSe layers is 9.32 Å, which is much larger than in bulk FeSe (5.5 Å) [21]. This

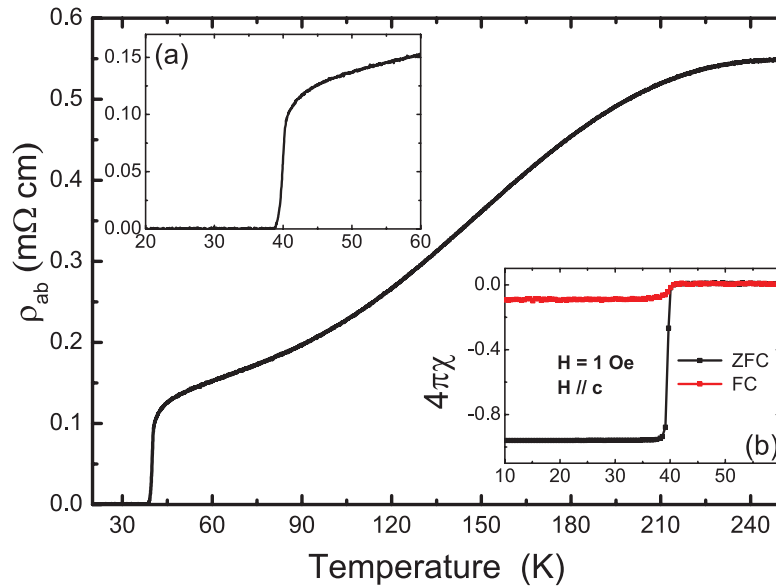


Figure 1. Temperature dependence of the in-plane electrical resistivity of FeSe1111 in zero field up to 250 K. Inset (a) shows a magnified view near T_c , inset (b) the magnetic susceptibilities for zero-field cooling (ZFC) and field cooling (FC, 1 Oe along the c axis).

signals a weak interaction between the two adjacent FeSe layers in FeSe1111 and an enhanced two-dimensional nature of the electronic structure compared to bulk FeSe. The phase diagram of FeSe1111 suggests that FeSe- and FeAs-based superconductors may share a common mechanism for superconductivity [21]. It further has been reported that FeSe1111 has only electron-like Fermi-surface pockets and might have an electronic origin of superconductivity in common with the single-layer FeSe/SrTiO₃ films [24].

As FeSe1111 is a single-phase bulk superconductor with a relatively high T_c and free from complications of phase separation and interface effects, studies of this material can be very important for unveiling the mechanism of high-temperature superconductivity in the Fe-based materials. As a basic parameter, the temperature dependence of the upper critical field, H_{c2} , reflects the underlying electronic structure responsible for superconductivity and provides valuable information on the microscopic origin of pair breaking. Thus, by measuring the temperature dependence of H_{c2} of FeSe1111 information on the superconducting pairing mechanism can be gained.

In this work, we present the temperature dependence of H_{c2} for magnetic fields applied along the c axis and in the ab plane for an FeSe1111 single crystal. H_{c2} was determined from magnetotransport measurements over a wide range of temperatures down to 1.4 K in static magnetic fields up to 14 T and pulsed magnetic fields up to 70 T.

2. Experiment

Single crystals of FeSe1111 were grown by a hydrothermal ion-exchange technique using a large insulating K_{0.8}Fe_{1.6}Se₂ crystal as a matrix. We studied four crystals from the same batch. As the results are very similar, here we only show the data from one crystal. The superconducting transition in the investigated crystal is clearly resolved at $T_c \approx 40$ K in the resistivity and magnetic susceptibility (figure 1). The sample shows

a very narrow superconducting transition width of less than 1 K as seen in the magnetic-susceptibility data (inset (b) of figure 1), reflecting a high crystal quality. A more detailed characterization of the material can be found in previous publications [21–23].

The resistivity in the ab plane (ρ_{ab}) was measured by a standard four-probe method with magnetic fields applied parallel to the ab plane and the c axis, respectively. The field-dependent resistivity ρ_{ab} was measured at different temperatures using a 70 T non-destructive pulsed magnet with a pulse duration of about 150 ms driven by a capacitor bank at the Dresden High Magnetic Field Laboratory (HLD) [25]. To minimize the self-heating effect in pulsed magnetic fields, the sample was cut to a size of about 2 mm × 0.5 mm × 0.1 mm. The applied current was 1 mA at a frequency of 10 kHz. The voltage was recorded by a digital oscilloscope, Yokogawa DL750, with a high sampling rate of 1 MS s⁻¹ and a resolution of 16 bit. After the pulse, the signal processing was performed by use of a lock-in software procedure. No obvious heating effects were observed as the resistance curves collected in up and down sweeps of the magnet are identical within error bars. The down-sweep branch of the pulse was used to determine ρ_{ab} and from that H_{c2} utilizing its long decay time (about 120 ms). In order to extract the temperature dependence of H_{c2} near T_c more accurately, the temperature dependence of ρ_{ab} was measured by use of a commercial Physical Property Measurement System (PPMS) with magnetic fields up to 14 T.

3. Results and discussion

Figure 2 shows the temperature dependence of ρ_{ab} of the FeSe1111 single crystal in magnetic fields from 0 to 14 T for $H||c$ and $H||ab$, respectively. The magnetic field shifts the zero-resistance state to lower temperature much faster for $H||c$ than for $H||ab$, implying a high anisotropy of H_{c2} close to T_c . The magnetic-field dependence of ρ_{ab} measured at different temperatures in pulsed magnetic fields up to 70

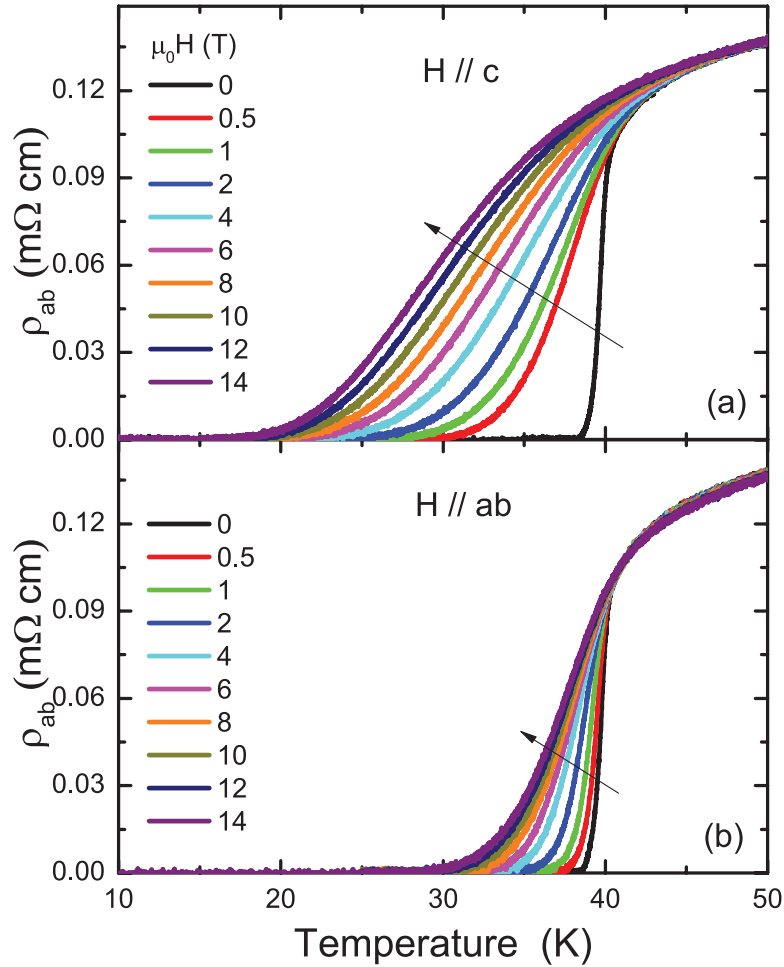


Figure 2. Temperature dependence of the in-plane electrical resistivity ρ_{ab} of FeSe1111 at fields $\mu_0H = 0, 0.5, 1, 2, 4, 6, 8, 10, 12$ and 14 T with (a) $H \parallel c$ and (b) $H \parallel ab$.

T for $H \parallel c$ and $H \parallel ab$ is shown in figures 3(a) and (b), respectively. Apparently, a stronger in-plane field ($H \parallel ab$) is needed to suppress superconductivity, consistent with the expected large electronic anisotropy in the layered FeSe1111 material. Similar anisotropies have been found for other Fe-based superconductors [26–34]. One can see that more than 60 T is needed to induce $\rho_{ab} > 0$ at 1.4 K for $H \parallel c$. For $H \parallel ab$ and $T = 24$ K, the maximum field of 70 T is just sufficient to leave the zero-resistance state. For lower temperatures $\rho_{ab} = 0$ up to highest fields.

For both field directions, clear field-induced broadenings of the resistive transitions are observed. This contrasts the behavior seen for Ba122 [28, 29, 35, 36], $\text{FeTe}_{0.6}\text{Se}_{0.4}$ [30] and LiFeAs [31], but is similar to the broadening found for $\text{NdFeAsO}_{0.7}\text{F}_{0.3}$ [33], $\text{SmFeAsO}_{0.85}$ and $\text{SmFeAsO}_{0.8}\text{F}_{0.2}$ [34], suggesting a wide vortex-liquid region in FeSe1111. It is known that for a broadened superconducting transition different criteria for the determination of the critical parameters can lead to different temperature dependences of H_{c2} [34]. We assume a similar scenario as was reported for $\text{SmFeAsO}_{0.85}$ and $\text{SmFeAsO}_{0.8}\text{F}_{0.2}$ [34]. For these superconductors the region around 10% of the normal-state resistance R_n is related to the vortex-liquid phase, while the region close to 90% of R_n is affected by superconducting fluctuations. Thus, we also

choose the temperature or field where R_n is reduced to 50% as the criterion to determine the $H_{c2} - T$ phase diagram.

The resulting critical fields $H_{c2}^{\parallel c}$ and $H_{c2}^{\parallel ab}$ are summarized in figure 4. The closed symbols are obtained from pulsed-field measurements utilizing magnetic-field scans (H scan), and the open symbols are obtained from PPMS measurements by use of temperature scans (T scan). The consistency of the data from those two different measurements proves the reliability of the results. $H_{c2}^{\parallel c}$ shows a quasilinear increase without a clear saturation at low temperatures, while $H_{c2}^{\parallel ab}$ has a tendency to saturate with decreasing temperature.

The data of $H_{c2}^{\parallel c}$ have a modest slope $-dH_{c2}^c/dT_c|_{T_c} = 2.29$ T K^{-1} close to T_c , but the data of $H_{c2}^{\parallel ab}$ are much steeper with a slope $-dH_{c2}^{ab}/dT_c|_{T_c} = 16.0$ T K^{-1} at T_c . From that, we can estimate the zero-temperature limits of the orbital critical fields by using the Werthamer–Helfand–Hohenberg (WHH) formula [37], $H_{c2\text{orb}}(0) = -0.69(dH_{c2}/dT)|_{T_c} T_c$. With $T_c = 40$ K, we estimate critical fields of $H_{c2\text{orb}}^c(0) = 63$ T and $H_{c2\text{orb}}^{ab}(0) = 440$ T. On the other hand, the Pauli-limiting field for a weakly coupled s -wave superconductor in the absence of spin-orbit scattering can be estimated by [38] $H_p(0)/T_c = 1.86$ T K^{-1} , resulting in $H_p(0) = 74.4$ T. Consequently, we expect for in-plane fields pronounced

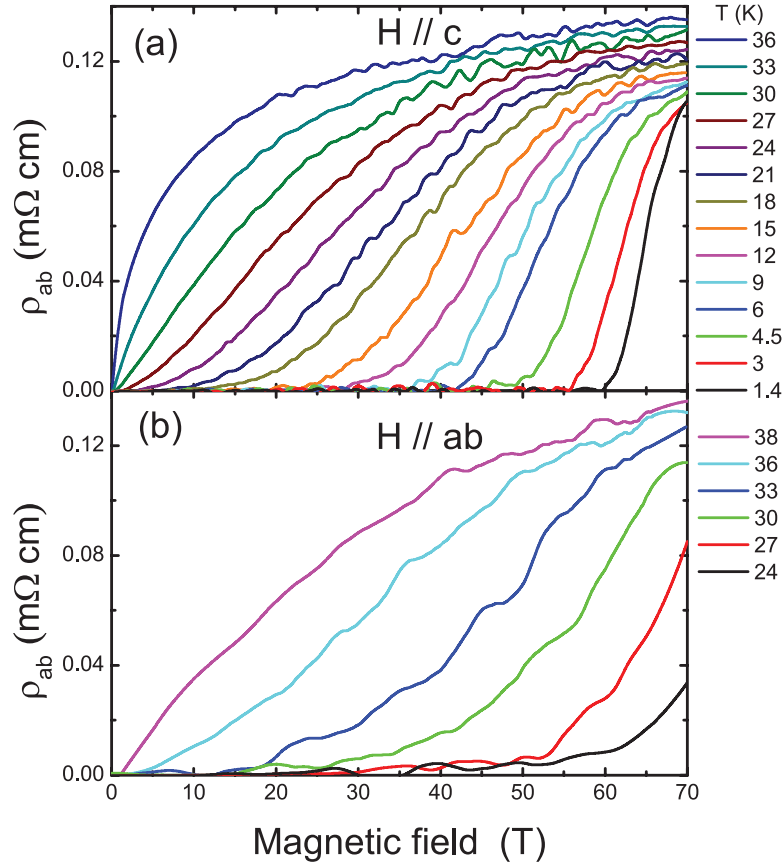


Figure 3. Magnetic-field dependence of the in-plane electrical resistivity ρ_{ab} of FeSe1111 at different temperatures with (a) $H\parallel ab$ and (b) $H\parallel c$ up to 70 T.

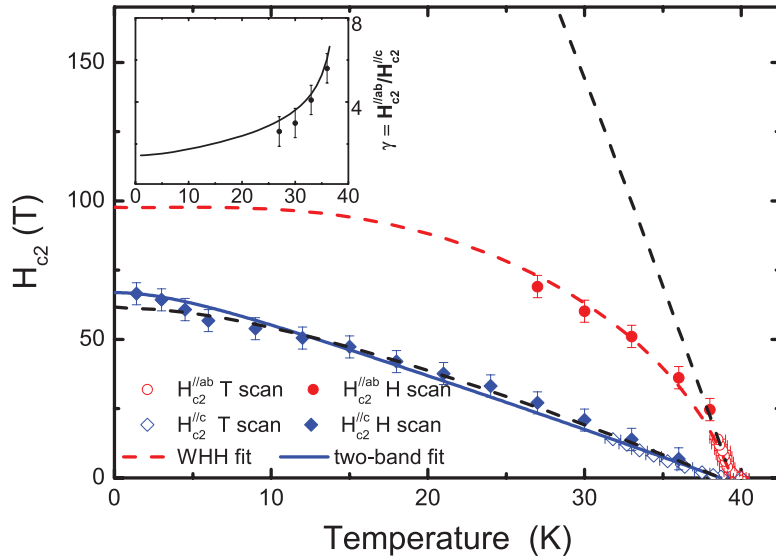


Figure 4. Temperature dependence of H_{c2} of FeSe1111 extracted from the magnetotransport measurements. The closed symbols are obtained from pulse-field measurements by scanning field (H scan), and the open symbols are obtained from PPMS measurements by scanning temperature (T scan). The red line shows a WHH fit with parameters $\alpha = 6.5$ and $\lambda_{so} = 0.32$ for $H_{c2}^{\parallel ab}$. The blue line is a two-band fit for $H_{c2}^{\parallel c}$ with parameters $D_1 = 4.9$ and $\eta = 0.36$. The dashed lines are the WHH predictions with $\alpha = 0$ and $\lambda_{so} = 0$ both for $H_{c2}^{\parallel ab}$ and $H_{c2}^{\parallel c}$. See equations (1) and (2) in the text. Inset: temperature dependence of the anisotropy parameter $\gamma = H_{c2}^{\parallel ab}/H_{c2}^{\parallel c}$.

Pauli-limiting effects leading to a curvature change of the $H_{c2}^{//ab}$ data with saturation towards zero temperature. Indeed, this fits nicely with our observation.

To quantitatively describe our results, a more complete theoretical treatment, taking into account both orbital pair-breaking and spin-paramagnetic effects, is needed. Therefore, we use the full WHH formula that incorporates the spin-paramagnetic effect via the Maki parameter α and spin-orbit effects via λ_{so} to describe the experimental H_{c2} data [37],

$$\ln \frac{1}{t} = \sum_{\nu=-\infty}^{\infty} \frac{1}{|2\nu+1|} - \left[|2\nu+1| + \frac{\bar{h}}{t} + \frac{(\alpha\bar{h}/t)^2}{|2\nu+1| + (\bar{h} + \lambda_{so})/t} \right]^{-1} \quad (1)$$

where $t = T/T_c$ and $\bar{h} = (4/\pi^2)[H_{c2}/|dH_{c2}/dT|_{T_c}]$. As shown by the red line in figure 4, the best fit ($\alpha = 6.5$ and $\lambda_{so} = 0.32$) can reproduce the experimental $H_{c2}^{//ab}$ data very well resulting in $H_{c2}^{//ab}(0) = 98$ T. However, for the other field direction the WHH fit (dashed black line) underestimates the low-temperature data of $H_{c2}^{//c}$ which is more important than the high-temperature data for Fe-based superconductors, even when considering the orbital pair breaking only ($\alpha = \lambda_{so} = 0$).

On the other hand, the quasilinear temperature dependence of $H_{c2}^{//c}$, which has been commonly observed in MgB₂ and some iron-based superconductors [26, 33, 34, 36], can be understood by an effective two-band model [39],

$$a_0[\ln t + U(h)][\ln t + U(\eta h)] + a_1[\ln t + U(h)] + a_2[\ln t + U(\eta h)] = 0. \quad (2)$$

The coefficients a_0 , a_1 , and a_2 are determined from the BCS coupling tensor $\lambda_{mm'}$ [39]. The function $U(x) = \psi(1/2+x) - \psi(1/2)$, where ψ is the di-gamma function. Other parameters are defined by $h = H_{c2}D_1/2\phi_0T$ and $\eta = D_2/D_1$, where ϕ_0 is the flux quantum and D_n is the electron diffusivity for the n th Fermi-surface sheet. Since the line shape mostly depends on the choice of D_1 and η rather than the coupling constants $\lambda_{mm'}$, we use $a_0 = 1$, $a_1 = 1.5$, and $a_2 = 0.5$, i.e. the same values as for the BaFe_{2-x}Ni_xAs₂ superconductors [36], and only tune D_1 and η to describe our $H_{c2}^{//c}$ data, where $\eta \neq 1$ means different intraband scattering on each Fermi sheet. The best fit with $D_1 = 4.9$ and $\eta = 0.36$ agrees very well with the $H_{c2}^{//c}$ data and gives $H_{c2}^{//c}(0) = 67$ T (blue line in figure 4). It is also possible to fit the $H_{c2}^{//ab}$ data with the two-band model, but that would introduce a much higher uncertainty in the obtained parameters because of the additional parameters to be used.

The anisotropy parameter $\gamma = H_{c2}^{//ab}/H_{c2}^{//c}$ is about 7 near T_c and decreases considerably towards lower temperatures (inset of figure 4). We calculated γ for the whole temperature range by using equations (1) and (2) with above fit results (line in the inset of figure 4). γ monotonically decreases with decreasing temperature and reaches about 1.5 for zero temperature. This weakened anisotropy at low temperatures, also observed in many other Fe-based superconductors [26–31, 33, 34, 40], is a

consequence of the Pauli-limiting effect that quickly becomes dominant for $H_{c2}^{//ab}$ somewhat below T_c .

4. Summary

In summary, we have constructed the $H_{c2} - T$ phase diagram for FeSe11111 with $T_c \approx 40$ K by use of electrical-transport measurements in magnetic fields up to 70 T aligned both within the ab plane and along the c axis. The quasilinear $H_{c2}^{//c}$ data can be described by an effective two-band model, whereas the $H_{c2}^{//ab}$ data follow the WHH model including orbital pair-breaking and spin-paramagnetic effects. The upper critical fields of FeSe11111 are determined as $H_{c2}^{//c}(0) = 67$ T and $H_{c2}^{//ab}(0) = 98$ T. The anisotropy of H_{c2} monotonically decreases from about 7 near T_c to 1.5 at 0 K due to the strong paramagnetic pair-breaking effects for in-plane magnetic fields.

Acknowledgments

We acknowledge the support of the HLD at HZDR, member of the European Magnetic Field Laboratory (EMFL). JY acknowledges the support of Outstanding technologist program of the Chinese Academy of Sciences. The work at IOP, CAS, is supported by NSFC (11574370 and 11274358).

References

- [1] Kamihara Y, Watanabe T, Hirano M and Hosono H 2008 *J. Am. Chem. Soc.* **130** 3296
- [2] Ren Z A et al 2008 *Chin. Phys. Lett.* **25** 2215
- [3] Hsu F C et al 2008 *Proc. Natl Acad. Sci.* **105** 14262–4
- [4] McQueen T M et al 2009 *Phys. Rev. B* **79** 014522
- [5] Dagotto E 2013 *Rev. Mod. Phys.* **85** 849
- [6] Guo J, Jin S, Wang G, Wang S, Zhu K, Zhou T, He M and Chen X 2010 *Phys. Rev. B* **82** 180520
- [7] Ying J J et al 2011 *Phys. Rev. B* **83** 212502
- [8] Li C H, Shen B, Han F, Zhu X and Wen H H 2011 *Phys. Rev. B* **83** 184521
- [9] Fang M, Wang H, Dong C, Li Z, Feng C, Chen J and Yuan H Q 2011 *Europhys. Lett.* **94** 27009
- [10] Wang Z, Song Y J, Shi H L, Wang Z W, Chen Z, Tian H F, Chen G F, Guo J G, Yang H X and Li J Q 2011 *Phys. Rev. B* **83** 140505
- [11] Li W et al 2012 *Nat. Phys.* **8** 126–30
- [12] Bao W 2015 *J. Phys.: Condens. Matter* **27** 023201
- [13] Wang Q-Y et al 2012 *Chin. Phys. Lett.* **29** 037402
- [14] He S et al 2013 *Nat. Mater.* **12** 605–10
- [15] Ge J-F, Liu Z-L, Liu C, Gao C-L, Qian D, Xue Q-K, Liu Y and Jia J-F 2015 *Nat. Mater.* **14** 285–9
- [16] Peng R et al 2014 *Phys. Rev. Lett.* **112** 107001
- [17] Lee J J et al 2014 *Nature* **515** 245–8
- [18] Lu X F et al 2014 *Nat. Mater.* **14** 325
- [19] Pachmayr U, Nitsche F, Luetkens H, Kamusella S, Brueckner F, Sarkar R, Klaus H-H and Johrendt D 2015 *Angew. Chem. Int. Ed.* **54** 293
- [20] Sun H et al 2015 *Inorg. Chem.* **54** 1958
- [21] Dong X et al 2015 *J. Am. Chem. Soc.* **137** 66
- [22] Dong X et al 2015 *Phys. Rev. B* **92** 064515

- [23] Wang C, Yi X, Qiu Y, Tang Q, Zhang X, Luo Y and Yu B 2016 *Supercond. Sci. Technol.* **29** 055003
- [24] Zhao L *et al* 2016 *Nat. Commun.* **7** 10608
- [25] Zherlitsyn S, Herrmannsdoerfer T, Skourski Yu, Sytcheva A and Wosnitza J 2007 *J. Low Temp. Phys.* **146** 719
- [26] Hunte F, Jaroszynski J, Gurevich A, Larbalestier D, Jin R, Sefat A S, McGuire M A, Sales B C, Christen D K and Mandrus D 2008 *Nature* **453** 903
- [27] Altarawneh M M, Collar K, Mielke C H, Ni N, Budko S L and Canfield P C 2008 *Phys. Rev. B* **78** 220505
- [28] Yuan H, Singleton J, Balakirev F F, Baily S A, Chen G, Luo J and Wang N 2009 *Nature* **457** 565
- [29] Kano M, Kohama Y, Graf D, Balakirev F, Sefat A S, McGuire M A, Sales B C, Mandrus D and Tozer S W 2009 *J. Phys. Soc. Japan* **78** 084719
- [30] Khim S, Kim J W, Choi E S, Bang Y, Nohara M, Takagi H and Kim K H 2010 *Phys. Rev. B* **81** 184511
- [31] Khim S, Lee B, Kim J W, Choi E S, Stewart G R and Kim K H 2011 *Phys. Rev. B* **84** 104502
- [32] Zhang J L, Jiao L, Balakirev F F, Wang X C, Jin C Q and Yuan H Q 2011 *Phys. Rev. B* **83** 174506
- [33] Jaroszynski J *et al* 2008 *Phys. Rev. B* **78** 174523
- [34] Lee H-S, Bartkowiak M, Park J-H, Lee J-Y, Kim J-Y, Sung N-H, Cho B K, Jung C-U, Kim J S and Lee H-J 2009 *Phys. Rev. B* **80** 144512
- [35] Wang Z S, Luo H Q, Ren C and Wen H H 2008 *Phys. Rev. B* **78** 140501
- [36] Wang Z *et al* 2015 *Phys. Rev. B* **92** 174509
- [37] Werthamer N, Helfand E and Hohenberg P 1966 *Phys. Rev.* **147** 295
- [38] Clogston A M 1962 *Phys. Rev. Lett.* **9** 266
- [39] Gurevich A 2003 *Phys. Rev. B* **67** 184515
- [40] Mun E D, Altarawneh M M, Mielke C H, Zapf V S, Hu R, Bud'ko S L and Canfield P C 2011 *Phys. Rev. B* **83** 100514